Chapter

Radiation Effect on Optical Properties of Bi-Related Materials Co-Doped Silica Optical Fibers

Jianxiang Wen, Ying Wan, Yanhua Dong, Yi Huang, Yanhua Luo, Gang-Ding Peng, Fufei Pang and Tingyun Wang

Abstract

Three kinds of Bi-related materials co-doped silica optical fibers (BRDFs), including Bi/Al, Bi/Pb, and Bi/Er co-doped fibers, were fabricated using atomic layer deposition (ALD) and modified chemical vapor deposition (MCVD). Then, the effect of irradiation on the optical properties of BRDFs was investigated. The experimental results showed that the fluorescence intensity, the fluorescence lifetime of BRDFs at the 1150 nm band, increased significantly with low-dose treatment, whereas it decreased with a further increase in the radiation dose. In addition, the merit M_{α} values of the BRDFs, a ratio of useful pump absorption to total pump absorption, decreased with an increase of the radiation doses. The Verdet constants of different doped fibers increased up to saturation level with increases in the radiation dose. However, for a Bi-doped fiber, its Verdet constant decreased and the direction of Faraday's rotation changed under low-dose radiation treatment. In addition, the Verdet constant increase of the Bi-doped silica fiber was much faster than that of other single mode fiber (SMF) and Pb-doped silica fibers treated with high-dose radiation. All of these findings are of great significance for the study of the optical properties of BRDFs.

Keywords: Bi-related materials, optical properties, gamma-ray radiation, silica optical fiber

1. Background and meaning

Bismuth oxide is an important material with many promising applications [1, 2]. In particular, bismuth-doped optical fibers, as a promising active medium for amplifying and lasing in the 1.1–1.8 μm range [3, 4], have been extensively studied, ever since their broadband near-infrared (NIR) fluorescence properties were first reported by Fujimoto et al. [1]. Thereafter, an amplification at the 1300 nm band in Bi-doped silica glass was realized [2] and an optical amplifier and fiber laser were achieved [4–6]. Previous investigations have demonstrated that the valence state of Bi ions varies in glass materials [7–11]. However, the valence conversion mechanism of Bi-related materials for silica optical fibers remains unclear.

In addition, the effects of radiation on the fluorescence properties of Bi-doped glass or optical fibers have been previously studied [12–18]. In Refs. [16–18], the

radiation-induced photoluminescence (PL) effect of Bi-doped silica optical fibers was investigated and the relationships between the radiation-induced optical properties and defect centers in Bi-doped silica fibers (BDFs) were reported. Moreover, the fluorescence intensity was enhanced by UV irradiation [11, 12]. Shen et al. [14] also reported fluorescence enhancement from exposing Bi-doped borosilicate glass to a radiation environment. The photo-bleaching effect on Bi-doped glass fiber with a 532-nm laser treatment was studied [15]. These results provide deeper insight into the nature and formation mechanism of PL [19]. Furthermore, the magneto-optical properties of the Bi-doped silica fibers were studied before and after irradiation, and radiation-induced magneto-optical phenomena were found [20–22]. Finally, thermal effects on the luminescence properties of Bi co-doped silica fibers were studied [23–25].

However, the nature of the NIR fluorescence properties in Bi-doped glass or silica optical fibers is still unclear. Although many studies have reported the luminescent properties of Bi co-doped fibers, there are few reports on the effect of irradiation on the optical properties of Bi-related co-doped silica optical fibers.

In this chapter, three kinds of Bi-related co-doped silica optical fibers, including Bi/Al, Bi/Pb, and Bi/Er co-doped fibers, are fabricated using atomic layer deposition (ALD) combined with a modified chemical vapor deposition (MCVD) process. The optical properties of bi-related materials co-doped silica optical fibers (BRDFs) that are influenced by irradiation are investigated, including luminescence, lifetime decay, magnetic-optical, and unsaturable absorption, and the changes in these optical properties are compared.

2. Fabrication of Bi-related co-doped silica optical fibers

Currently, the fabrication technologies of different doped fibers such as rare earth-doped fibers mainly use a solution-doping chemical vapor deposition technique. However, the technology lacks uniformity and consistency, and doping materials are easily volatilized and form clusters in a high-temperature environment, which limits the excellent performance of the fabricated doped fibers. Recently, a novel doping method, ALD technology, has been developed. It is not only an advanced deposition technique [5, 26–30] that allows for ultrasmall dopants of a few nanometers to be deposited in a precisely controlled way but also a chemical vapor deposition technique based on the sequential use of self-terminating gas–solid reactions. In particular, the novel technology involves a self-limiting surface reaction, whose advantages include a low-temperature process, good uniformity, favorable dispersibility, high doping concentration, and wide range of materials used. To date, there have been only a few reports [30–34] regarding the preparation of rare earth optical fibers by ALD.

ALD technology typically involves a cycle of four steps that is repeated as many times as necessary to achieve the required doping concentrations. As an example, we perform ALD on Al_2O_3, using $Al_2(CH_3)_3$ (Trimethylaluminum, TMA) and H_2O as the reactants. The detailed deposition process is shown in **Figure 1**. **Step 1:** A pulse precursor vapor of TMA reacts with the inner surface of the substrate tube. With the optimized choice of precursors and reaction conditions, the reaction of this step is self-limiting. **Step 2:** Purging all residual precursors and reaction products. **Step 3:** Low damage by remote exposure of the surface to reactive oxygen radicals, where these radicals oxidize the inner surface and remove surface ligands. This reaction is also self-limiting because of the limited number of surface ligands. **Step 4:** Reaction products are purged from the chamber. Only Step 3 varies, between H_2O and O_2 plasma by thermal processing. As each cycle of the ALD process deposits

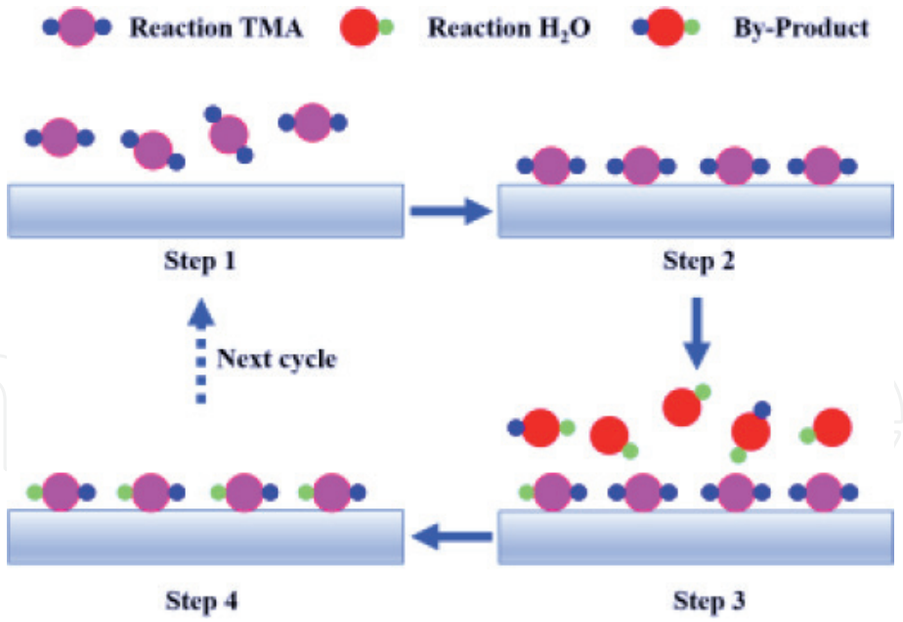

Figure 1.
Specific process of ALD technology deposition.

a layer of sub-angstrom thickness, the atomic scale ranges of deposition can be controlled through the process.

The reaction of $X(thd)_3$ (X: metal ions, such as Bi, Pb, and Er; thd: 2,2,6,6-tetramethyl-3,5-heptanedionato) and H_2O can be described by Eqs. (1)–(3) [35]. The whole reaction can be written as follows:

$$2X(thd)_3 + 3H_2O \rightarrow X_2O_3 + 6H - thd \quad (1)$$

which involves two processes: process A in Eq. (2) is the hydroxyl on silicon reacting with the X source to obtain Si-O-$X(thd)_2$; process B is obtaining Si-O-$X(OH)_2$ by the reaction in Eq. (3) of H_2O and Si-O-$X(thd)_2$ with the termination of —OH groups. On repeating the ABAB (A and B represent different reaction processes, respectively) operations, an X-doped layer with the desired thickness is obtained. Similarly, Al_2O_3 can be deposited using these following analogous reactions.

$$A: Si - OH + X(thd)_3 \rightarrow Si - O - X(thd)_2 + H - thd \quad (2)$$

$$B: Si - O - X(thd)_2 + 2H_2O \rightarrow Si - O - X(OH)_2 + 2H - thd \quad (3)$$

The fabrication process of the BRDFs can be divided into four steps, as shown in **Figure 2**. First, a porous soot layer is deposited inside the silica substrate tube using

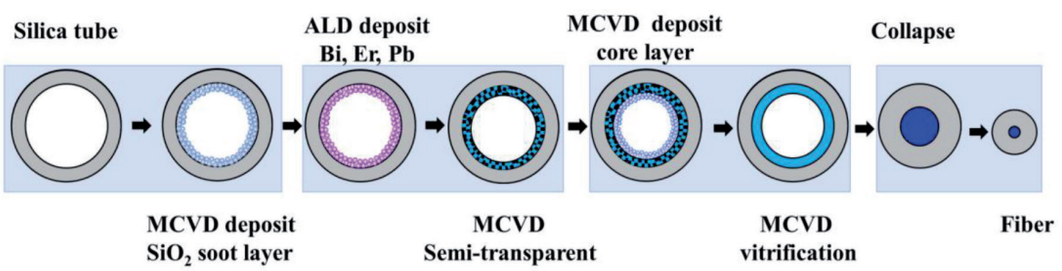

Figure 2.
Fabrication process of the BRDFs based on ALD + MCVD technology.

the MCVD method. In this process, chemical reactions in the gas phase generate a fine soot of silica that coats the inner surface of the substrate tube, which is then sintered into a semi-clear soot layer. Second, Bi, Pb, or Er ions are introduced on the surface of the porous soot layer using the ALD technique (TFS-200, Beneq, Finland). This results in the formation of bismuth oxide, lead oxide, and erbium oxide with the precursors of bis (2, 2, 6, 6-tetra-methyl-3, 5-heptanedionato) bismuth (III) ($Bi(thd)_3$), bis (2, 2, 6, 6-tetra-methyl-3, 5-heptanedionato) lead (III) ($Pb(thd))_3$, and bis (2, 2, 6, 6-tetra-methyl-3, 5-heptanedionato) erbium (III) ($Er(thd))_3$ (supplied by Shanghai J&K Scientific Ltd), respectively. They mainly react with water or ozone to form the metal oxidation layer, the O_3 that originated from the O_2. Third, germanium oxide is doped into the fiber preform core by the MCVD process, and then a Bi-related co-doped optical fiber preforms with a Ge-doped higher index core that is formed by collapsing on an MCVD lathe heated by a high-temperature oxyhydrogen flame. Finally, the preform is drawn into a doped optical fiber with a Bi-related material.

3. Effect of radiation on optical properties

For optical fiber material, a perfect structure is visualized as a co-doped ion random network of SiO_4 tetrahedrons joined at the corner, and different ions are doped into irregular vitreous silica, forming a stable network structure [36]. It is important to accumulate further knowledge regarding the influence of radiation on optical fiber materials, including material network structures, defect centers, and optical properties. Radiation as an effective method can induce changes in the optical properties of materials. It mainly involves the process of high-energy particles interacting with fiber materials, including the photoelectric effect, the Compton effect, the electron pair effect, and more. For BRDFs, irradiation significantly improves their optical properties, which mainly accounts for the variation in the valence states of Bi (Bi^{5+}, Bi^{2+}, Bi^{+}, Bi^{0}, defect centers, Bi clusters, $Bi^{2-}{}_2$ dimers, or Bi atoms). Here, gamma rays are selected as the irradiation source, mainly due to their short wavelength and strong penetrating ability. The effects of gamma ray irradiation on the optical properties of BRDFs, including Bi/Al co-doped silica fibers (BADFs), Bi/Er co-doped silica fibers (BEDFs), and Bi/Pb co-doped silica fibers (BPDFs), are investigated.

3.1 Radiation effect on luminescence characteristics

The radiation-induced PL properties of BADFs were investigated in [19]. The PL spectra in the inset of **Figure 3** reveal two emission bands at approximately ~1150 and ~ 1410 nm, corresponding to the aluminum-related Bi active center (BAC-Al) and the silicon-related Bi active center (BAC-Si), respectively. **Figure 3** illustrates that the fluorescence intensities of BAC-Al increased by 0.73, 2.25, and 1.35 dB at 1150 nm with 1.0, 2.0, and 3.0 kGy of irradiation, respectively. The fluorescence intensities of BAC-Al in the BADF samples increased with the increase in radiation dose (0–2.0 kGy) and then decreased when the radiation dose exceeded 2 kGy. Moreover, the change in the fluorescence intensity of BAC-Si trended similar to that of BAC-Al; however, the fluorescence intensity of BAC-Si increased considerably more. Furthermore, the fluorescence intensity of BAC-Si was approximately four times stronger than that of the unirradiated fiber sample.

For BEDF, five BEDF samples were irradiated with cumulative doses of approximately 0.3, 0.5, 0.8, 1.5, and 3.0 kGy at room temperature. The radiation dose rate was 800 Gy/h. Under excitation at 980 nm (pump power is 1.8 mW),

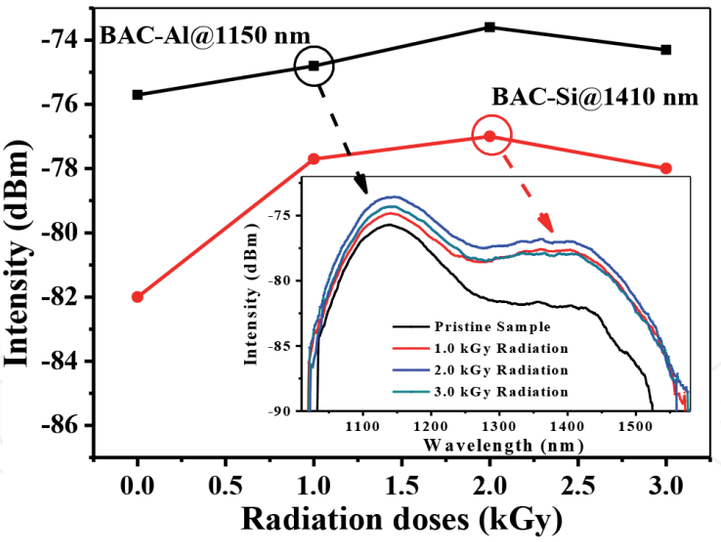

Figure 3.
Fluorescence intensity of BAC-Al and BAC-Si as a function of radiation dose; inset are the PL spectra of the BADF samples before and after γ-ray irradiation.

the fluorescence spectra of BEDF samples were measured, as shown in **Figure 4**. For BAC-Al, as the radiation dose was increased, the fluorescence intensity first increased and then decreased. With a 0.3 kGy dose of irradiation, the fluorescence intensity of BAC-Al in the BEDF sample is slightly higher than that of the pristine fiber, as shown in **Figure 4(a)**. However, when the radiation dose was less than

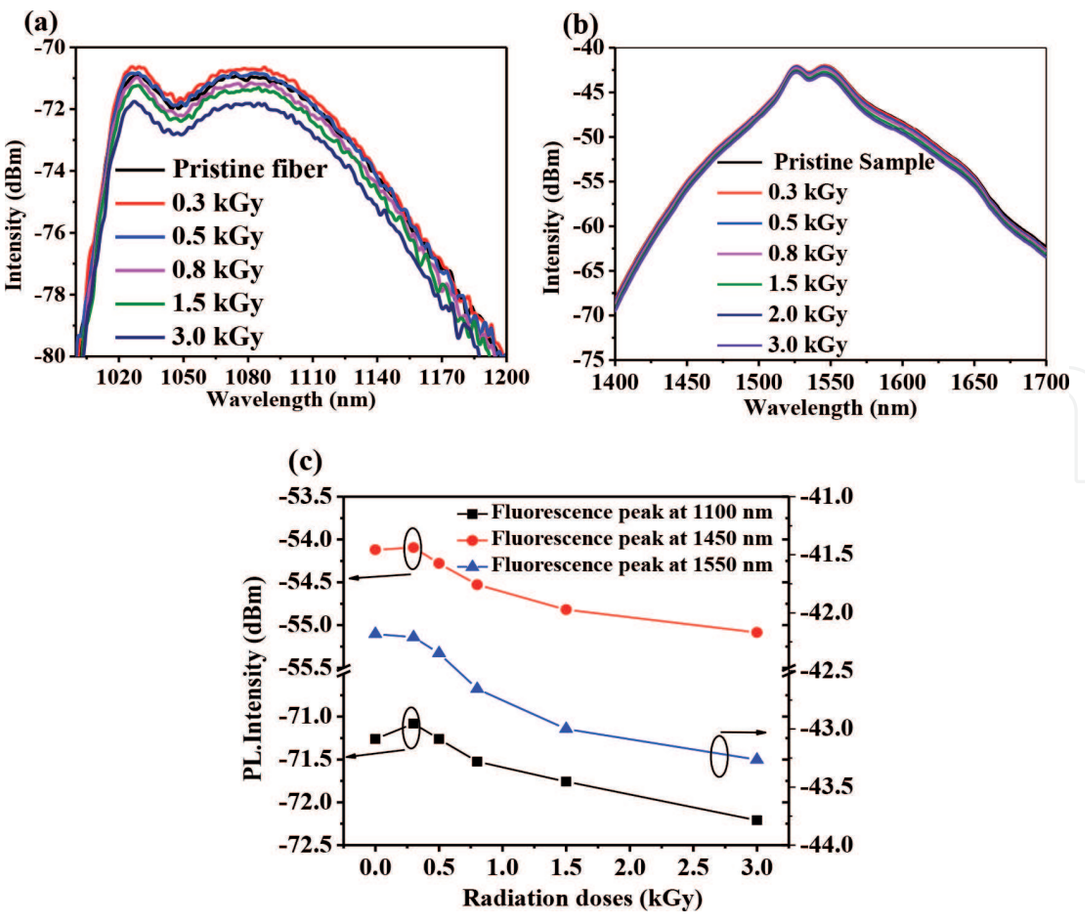

Figure 4.
Fluorescence spectra of BEDF samples at different bands with different radiation doses. (a) 1100, (b) 1550 nm, and (c) the variations of the fluorescence intensity at 1100, 1450, and 1550 nm.

0.5 kGy, the fluorescence intensity of BAC-Al was significantly lower than that of the pristine fiber. In addition, the fluorescence intensity of BAC-Si in BEDF showed the same trend in **Figure 4(c)** (red curve). The fluorescence of Er ions at 1550 nm was also observed, as shown in **Figure 4(b)**. For Er ions, the fluorescence intensity decreased with an increase in the radiation dose and fluorescence enhancement at low-dose radiation (<0.5 kGy) such as Bi ions did not appear..

For BPDF, five BPDF samples were irradiated with cumulative doses of approximately 0.3, 1.0, 1.5, 2.0, and 3.0 kGy at room temperature. The radiation dose rate was 800 Gy/h, which is the same as in the other experiment. The fluorescence spectra of BPDFs at different doses under 830 nm pumping are shown in **Figure 5(a)**. Comparing the PL spectra before and after irradiation, the shape did not change significantly. The fluorescence spectra of the fiber samples range from 1100 to 1600 nm with a peak at 1420 nm, which is derived from BAC-Si. The change in the fluorescence peak of BAC-Si is shown in **Figure 5(b)**. With an increase in the radiation dose, the fluorescence intensities of BAC-Si first increased and then decreased with a further increase in the radiation dose. Moreover, when the radiation dose was 1.5 kGy, the fluorescence intensity of BAC-Si was two times that of the unirradiated BPDF. That is to say, low-dose irradiation can promote the formation of BAC-Si, enhancing the fluorescence intensity. For radiation doses up to 3.0 kGy, the fluorescence intensity of BAC-Si was still higher than that of untreated fiber. This indicated that the BPDF samples had a certain degree of radiation resistance, which has great potential for photonic applications of optical fiber amplification devices in harsh radiation environments.

3.2 Radiation effect on fluorescence lifetime

The luminescence decay curves of the Bi-related active centers in BEDFs and BPDFs were measured using a fluorescence spectrophotometer (Edinburgh FLS-980, England) equipped with an nF900 flash lamp. The fluorescence lifetime decay curves of BAC-Al in BEDF samples before and after radiation are shown in **Figure 6(a)**. In order to compare the fluorescence decay curves of the BEDF samples with different radiation doses, a single exponential function was used to fit them. The relationship between fluorescence lifetime and radiation dose is shown in **Figure 6(b)**. When the radiation doses were 0, 0.3, 0.5, 0.8, 1.5, and 3 kGy, the fluorescence lifetimes of BAC-Al were 564, 599, 585, 560, 559, and 553 μs, respectively. These results demonstrated that their lifetimes increased at low radiation doses (0–0.3 kGy) that were increasing, whereas at higher radiation doses (0.5–3 kGy), their lifetimes were decreased.

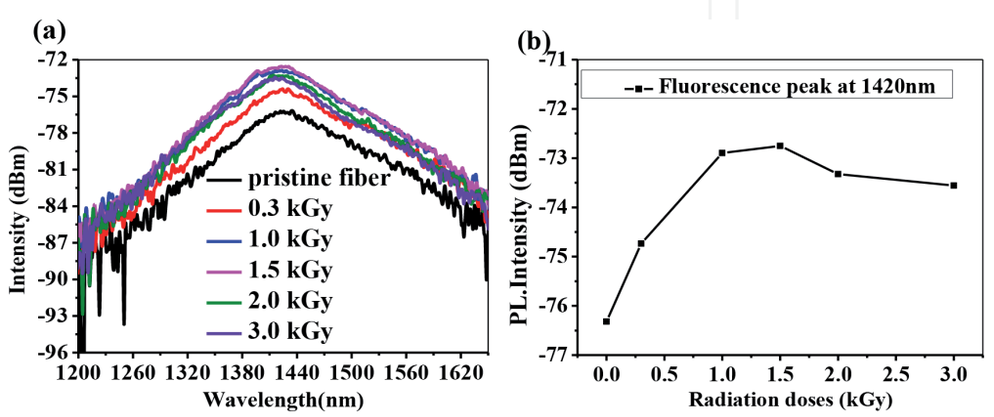

Figure 5.
(a) PL spectra of BPDF samples with different radiation doses and (b) variation of the fluorescence intensity at 1420 nm.

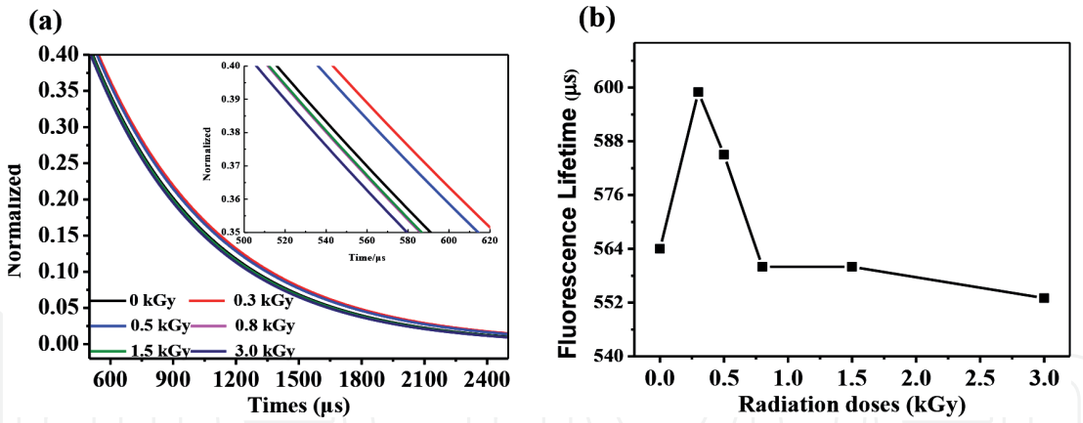

Figure 6.
(a) Luminescence decay curves with different radiation doses and (b) variation in the fluorescence lifetime.

For comparative analysis, the fluorescence lifetime of the Er^{3+} ions at 1534 nm was also measured, as shown in **Figure 7(a)**; when the radiation doses were 0, 0.3, 0.5, 0.8, 1.5, and 3 kGy, the fluorescence lifetimes of the Er^{3+} ions were 11.26, 11.13, 11.11, 11.10, 10.73, and 10.23 ms, respectively. The fluorescence lifetimes of Er^{3+} ions decreased with increasing of radiation doses, as shown in **Figure 7(b)**.

For the BPDF samples, the luminescence decay curves of BAC-Al are presented in **Figure 8(a)**. The single exponential function is a close fit. The luminescence lifetimes of BAC-Al were 740, 699, 573, and 500 μs for radiation doses of 0, 0.3, 1.0, and 3.0 kGy, respectively. Further, under the radiation conditions, the lifetimes of BAC-Al decreased rapidly, as shown in **Figure 8(b)**. It is inferred that the radiation increases the probability of the non-radiative transition, which may be attributed to the faster process whereby the electron in the excited state returns to the ground state or to the role of lead ions. To confirm this hypothesis, a more detailed experiment is required in the future.

3.3 Effect of radiation on unsaturable absorption characteristics

Unsaturable pump absorption (α_{us}) is ideally determined by the direct measurement of the remaining absorption of pump light. The saturable pump absorption (α_s), which is a measure of the effective pump absorption of the fiber used for the radiative emission, decreases with the increasing pump power. The pump absorption consists of α_{us} and α_s. In fact, we focus more on the merit M_α, defined as

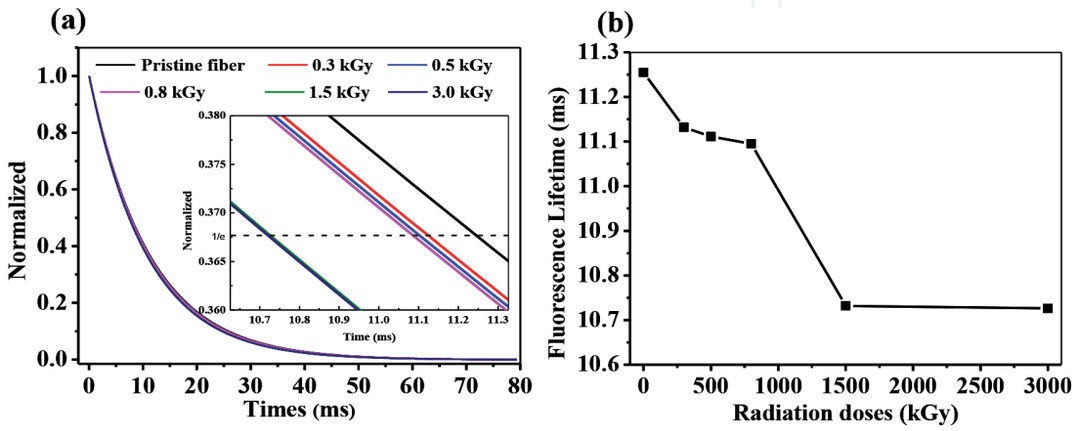

Figure 7.
(a) Luminescence decay curves of Er^{3+} active center in BEDF with different radiation doses and (b) variation of the fluorescence lifetime.

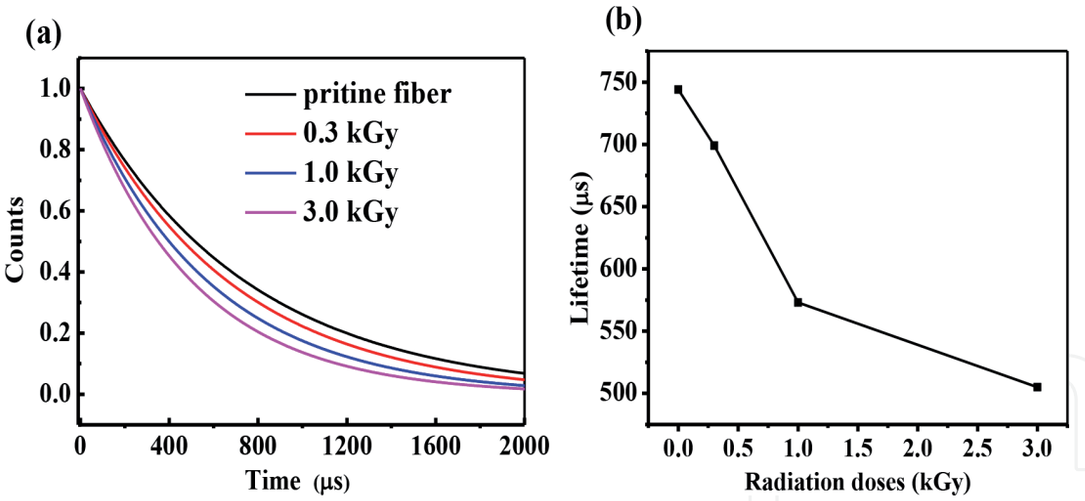

Figure 8.
(a) Luminescence decay curves of BAC-Al in BPDF samples with different radiation doses and (b) variation of the fluorescence lifetime.

$M_\alpha = \alpha_s / (\alpha_s + \alpha_{us})$, which represents the ratio of useful pump absorption, α_s, to the total pump absorption at the pump wavelength. This fraction is a key indicator of useful pump absorption and has a direct correlation to laser efficiency. Here, the unsaturable absorption characteristics of BEDFs at 980 nm before and after irradiation were investigated, as shown in **Figure 9(a)**. When the radiation doses were 0, 0.3, 0.5, 0.8, 1.5, and 3 kGy, the α_{us} values of the BEDF were 40.6, 37.0, 40.7, 43.5, 46.8, and 49.6 dB/m, respectively. As the radiation dose increased, α_{us} first decreased and then increased, as shown in **Figure 9(b)**. According to the relationship between $\alpha_{\mu s}$ and the radiation dose, the decrease of $\alpha_{\mu s}$ in the sample at a low radiation dose (0.3 kGy) may be attributed to the local structural change of Bi ions. Moreover, when the radiation dose was below 3.0 kGy, the α_s of the BEDF (3.6 dB/m) was smaller than that of the unirradiated BEDF. At the same time, their corresponding M_α values were also calculated as 58.6%, 57.5%, 54.8%, 53.3%, 52.2%, and 50.2%. Hence, the M_α of BEDF continuously decreased with an increase in the radiation dose.

The unsaturable absorption characteristics of the BPDF and Bi-doped silica fibers are shown in **Figure 10**. The unsaturable absorption of the Bi-doped silica fiber (α_{us1}) and the Pb/Bi co-doped silica fiber (α_{us2}) at 830 nm were approximately 18 and 8 dB/m, respectively, and their corresponding saturable absorptions were 72 dB/m (α_{s1}) and 45 dB/m (α_{s2}), respectively.

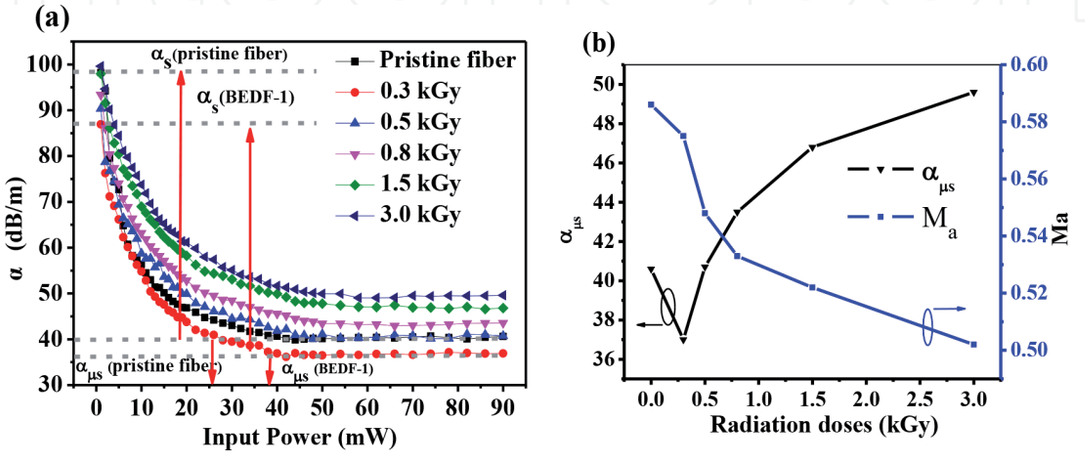

Figure 9.
(a) Unsaturable absorption characteristic of BEDF samples with different radiation doses and (b) variation of the α_{us} and M_α.

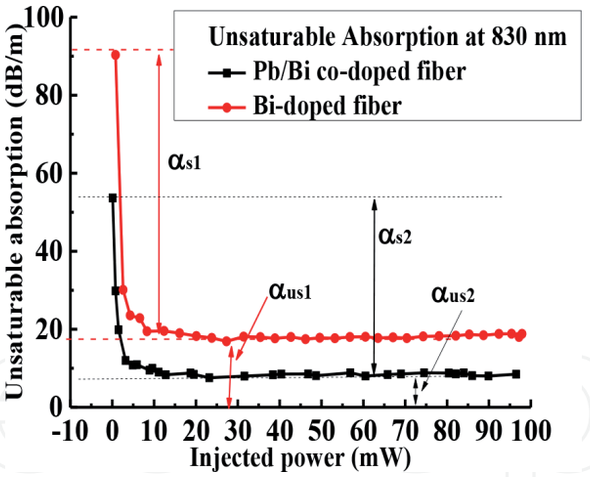

Figure 10.
Unsaturable absorption characteristic of Pb/Bi co-doped fiber (black curve) and Bi-doped fiber (red curve) at 830 nm.

The derived merit M_α of the Pb/Bi co-doped silica fiber was approximately 85.1%, which was larger than that of the Bi-doped silica fiber (80.0%). A high merit M_α meant that a large proportion of the pump photons would participate in the excitation of the active ions, promoting the desirable luminescence process at the corresponding bands. As such, the larger the M_α value, the higher the laser efficiency. Compared with the fiber-doped Bi ions only, the Pb/Bi co-doped silica fiber exhibited improved unsaturable characteristics. This would be beneficial for fiber lasers and amplifiers.

After the BPDF samples were treated with different radiation doses, the unsaturable absorption characteristics were measured as shown in **Figure 11(a)**, and both α_{us} and α_s changed significantly. With an increase in radiation dose, α_{us} trended with a gradual increase, whereas α_s decreased and exhibited a small fluctuation. Furthermore, M_a trended similar to α_s, as shown in **Figure 11(b)**. For the BPDF, the radiation effect on α_{us} was small, similar to the effect of radiation on the fluorescence lifetime of the Er^{3+} ions.

3.4 Effect of radiation on magnetic-optical property

To further study the influence of radiation on the characteristics of Bi ions, the effect of radiation on the magnetic-optical properties of the Bi-doped silica fiber (BDF) was investigated by comparing it with other silica fibers, such as SMF and Pb-doped silica fiber.

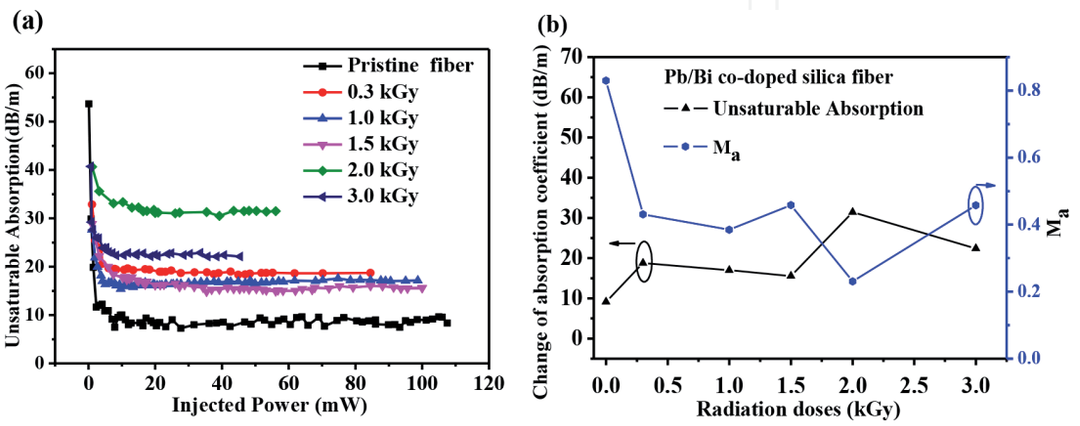

Figure 11.
(a) Unsaturable absorption characteristics of BPDF at 830 nm with different radiation doses and (b) unsaturated absorption coefficient and M_α value with the function of radiation dose.

The Faraday rotation degree of the BDF in different magnetic fields ranging from 0 to 118 mT was measured. The slope of the Faraday rotation curve, marked as β_i, where i = 1–7, in **Figure 12(a)**, determined the Verdet constants of the corresponding fiber samples. The Faraday rotations of the fiber samples were proportional to the intensity of the applied magnetic field. The slope of the rotation angle of BDF (β_2) before irradiation was larger than that of SMF (β_1). After the irradiation, the trend of the slope of the rotation angle changed from β_2 to β_4 clockwise, and then from β_5 to β_7 anticlockwise. The Verdet constant (1.64 rad/(Tm)) of the BDF before irradiation is 26.0% larger than that of SMF (1.29 rad/(Tm)), and the Verdet constant value is positive, indicating that the BDF material has diamagnetic properties. After radiation, the Verdet constant of the SMF increased with increasing radiation doses, as shown in **Figure 12(b)**; however, those of the BDF decreased at low radiation doses (<0.3 kGy). In particular, after 0.3 kGy of irradiation, the Verdet constant of the BDF became negative, showing that the BDF material has a paramagnetic property. Its Verdet constant value was positive and increased with the increase in radiation doses from 0.5 to 3 kGy. The Verdet constant of the BDF after 3.0 kGy of irradiation became 1.87 rad/(Tm), which is 23.84% larger than that of SMF with 1.51 rad/(Tm) and 44.96% larger than that of SMF without radiation.

For the irradiated SMF and Pb-doped silica fibers, their Verdet constants always increased with an increase in the radiation dose, as shown by the red and black curves in **Figure 13**. With a further increase in radiation doses, the Verdet constant of the SMF became essentially constant, which may be due to the fact that the concentration of Ge-related defect centers induced by radiation tended to be saturated. For the Pb-doped silica fiber, the Verdet constant also increased with an increase in the radiation dose (0–1.5 kGy). The Verdet constant of the Pb-doped silica fiber was higher than that of the SMF. This result indicated that gamma-ray radiation enhanced the Verdet constants of the fiber samples, especially for Pb-doped silica fibers. Irradiation not only induced Ge- and Si-related defect centers such as Si′, Ge′ color centers, but also led to new Pb-related defect centers in the Pb-doped silica fibers. These defect centers increased the electron transition probability of Pb^{2+} in $^1S_0 \rightarrow {}^1P_1$ and contributed further to the orbital electron spin. This may be why the increase of the Verdet constant for Pb-doped silica fiber is faster than that for the SMF with an increase in the radiation dose (1.5–2.5 kGy). Therefore, it is supposed that gamma rays improve the magneto-optical properties of fibers.

For the BDF irradiation, with the increase in the radiation dose, the Verdet constant of the BDF decreased first and then increased. In particular, under

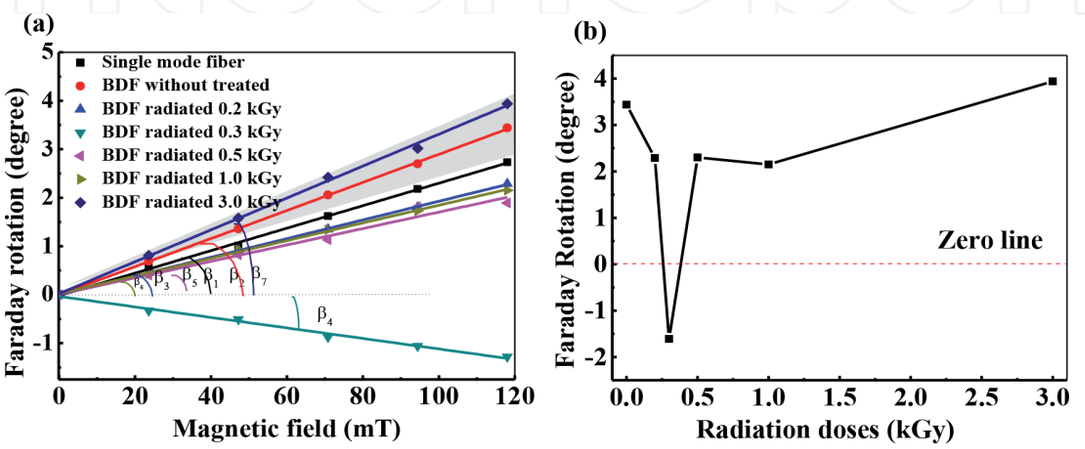

Figure 12.
Relationship between Faraday rotation and (a) magnetic field density and (b) radiation doses.

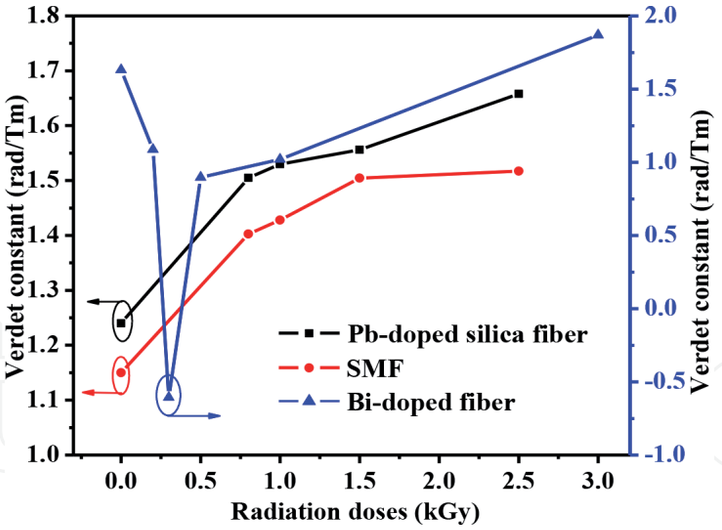

Figure 13.
Verdet constants of Bi-doped silica fiber, Pb-doped silica fiber, and SMF with different radiation doses.

0.3 kGy, the Verdet constant had a negative value, as shown by the blue curve in **Figure 11**. The change in the Verdet constant may mainly result from Bi ions, which present the formation of multiple valence states in the fiber, such as Bi^{0}, Bi^{1+}, Bi^{2+}, Bi^{3+}, and Bi^{5+}. Furthermore, among various valence states, the conversion may be possible under radiation treatment. These different valence states have different outer electronic shell structures. Bi^{3+} ($6s^{2}$) and Bi^{5+} ($5d^{10}$) ions, which have no unpaired electrons in their outer electronic shells, showed diamagnetic properties. In contrast, Bi^{0} ($6s^{2}6p^{3}$), Bi^{+} ($6s^{2}6p^{2}$), and Bi^{2+} ($6s^{2}6p^{1}$) showed paramagnetic properties because of unpaired electrons in the 6p layer, contributing to the intrinsic magnetic moment. These detailed results have already been reported in [22, 37]. Furthermore, the Verdet constant increase of the Bi-doped silica fiber was faster than that of the SMF and Pb-doped silica fiber with the increase in the radiation dose (1.5–2.5 kGy). Therefore, it is believed that gamma rays clearly improve the magneto-optical properties of the BDF.

4. Conclusion

In this chapter, certain types of BRDFs, including Bi/Al, Bi/Pb, and Bi/Er co-doped optical fibers, were fabricated using the ALD and MCVD process. Then, the radiation effects on their optical properties were investigated. The fluorescence intensity and fluorescence lifetimes of the BRDFs at 1150 nm with low-dose radiation increased significantly, whereas they decreased with a further increase in the radiation dose. The merit M_{α} values of the BRDFs, a ratio of useful pump absorption to total pump absorption, decreased with an increase in the radiation doses. However, the Verdet constants in different doped fibers increased and reached saturation with the increasing radiation dose. The incremental increases of the Verdet constants for the Pb-doped and Bi-doped fibers were faster than those for the SMF with an increase in the radiation dose (1.5–2.5 kGy). Moreover, the Verdet constant decreased and the direction of Faraday's rotation changed at low radiation doses. Hence, the increase in the Verdet constant increase for BDF is much faster than that of other fiber samples treated with high-dose radiation. All these results are of great significance for the study of the optical properties of BRDFs.

Funding

This work is supported by Natural Science Foundation of China (Grant Nos. 61520106014, 61975113, 61935002, and 61675125) and the Pre-Research Fund Project (6140414030203).

Author details

Jianxiang Wen[1*], Ying Wan[1], Yanhua Dong[1], Yi Huang[1], Yanhua Luo[2], Gang-Ding Peng[2], Fufei Pang[1] and Tingyun Wang[1]

1 Key Lab of Specialty Fiber Optics and Optical Access Networks, School of Communication and Information Engineering, Shanghai Institute for Advanced Communication and Data Science, Shanghai University, Shanghai, China

2 Photonics and Optical Communications, School of Electrical Engineering and Telecommunications, University of New South Wales, Sydney, NSW, Australia

*Address all correspondence to: wenjx@shu.edu.cn

References

[1] Fujimoto Y, Nakatsuka M. Infrared luminescence from bismuth-doped silica glass. Japanese Journal of Applied Physics. 2001;**40**(3B):L279-L281

[2] Fujimoto Y. Local structure of the infrared bismuth luminescent center in bismuth-doped silica glass. Journal of the American Ceramic Society. 2010;**93**(2):581-589

[3] Firstov S, Alyshev S, Melkumov M, R iumkin K, Shubin A, Dianov E. Bismuth-doped optical fibers and fiber lasers for a spectral region of 1600-1800 nm. Optics Letters. 2014;**39**(24):6927-6930

[4] Dianov EM. Amplification in extended transmission bands using bismuth-doped optical fibers. Journal of Lightwave Technology. 2013;**31**(4):681-688

[5] Razdobreev I, Bigot L, Pureur V, Favre A, Bouwmans G, Douay M. Efficient all-fiber bismuth-doped laser. Applied Physics Letters. 2007;**90**(3):031103

[6] Bufetov IA, Dianov EM. Bi-doped fiber lasers. Laser Physics Letters. 2009;**6**(7):487-504

[7] Zheng JY, Peng MY, Kang FW, Cao RP, Ma ZJ, Dong GP, et al. Broadband NIR luminescence from a new bismuth doped $Ba_2B_5O_9Cl$ crystal: evidence for the Bi^0 model. Optics Express. 2012;**20**(20):22569-22578

[8] Zhang LL, Dong GP, Wu JD, Peng MY, Qiu JR. Excitation wavelength-dependent near-infrared luminescence from Bi-doped silica glass. Journal of Alloys and Compounds. 2012;**531**:10-13

[9] Sokolov VO, Plotnichenko VG, Dianov EM. Origin of broadband near-infrared luminescence in bismuth-doped glasses. Optics Letters. 2008;**33**(13):1488-1490

[10] Ren JJ, Qiu JR, Chen DP, Wang C, Jiang XW, Zhu CS. Infrared luminescence properties of bismuth-doped barium silicate glasses. Journal of Materials Research. 2007;**22**(7):1954-1958

[11] Xia H, Wang X. Near infrared broadband emission from Bi^{5+}-doped Al_2O_3-GeO_2-X (X=Na_2O,BaO,Y_2O_3) glasses. Applied Physics Letters. 2006;**89**:051917

[12] Ban C, Bulatov LI, Dvoyrin VV, Mashinsky VM, Limberger HG, Dianov EM. Infrared luminescence enhancement by UV-irradiation of H_2-loaded Bi-Al-doped fiber. In: European Conference on Optical Communication, 35th ECOC. Vienna, Austria: IEEE; 2009. p. 2

[13] Violakis G, Limberger HG, Mashinsky VM, Dianov EM. Dose dependence of luminescence increase in H_2-loaded Bi-Al co-doped optical fibers by cw 244-nm and pulsed 193-nm laser irradiation. In: Optical Fiber Communication Conference, OFC. California, United States: IEEE; 2013. P. OTh4C.2

[14] Shen W, Ren J, Baccaro S, Cemmi A, Chen GR. Broadband infrared luminescence in γ-ray irradiated bismuth borosilicate glasses. Optics Letters. 2013;**38**(4):516-518

[15] Firstov S, Alyshev S, Khopin V, Melkumov M, Guryanov A, Dianov E. Photobleaching effect in bismuth-doped germanosilicate fibers. Optics Express. 2015;**23**(15):19226-19233

[16] Ou Y, Baccaro S, Zhang Y, Yang Y, Chen G. Effect of gamma-ray irradiation on the optical properties of PbO-B_2O_3-SiO_2 and Bi_2O_3-B_2O_3-SiO_2 glasses. Journal

of the American Ceramic Society. 2010;**93**(2):338-341

[17] Elbatal FH, Marzouk MA, Abdel-Ghany AM. Gamma rays interaction with bismuth borate glasses doped by transition metal ions. Journal of Materials Science. 2011;**46**(15):5140-5152

[18] Girard S, Kuhnhenn J, Gusarov A, Brichard B, Van Uffelen M, Ouerdane Y, et al. Radiation effects on silica-based optical fibers: Recent advances and future challenges. IEEE Transactions on Nuclear Science. 2013;**60**(3):2015-2036

[19] Wen JX, Liu WJ, Dong YH, Luo YH, Peng GD, Chen N, et al. Radiation-induced photoluminescence enhancement of Bi/Al-codoped silica optical fibers via atomic layer deposition. Optics Express. 2015;**23**:29004-29013

[20] Guo Q , Wen JX, Huang Y, Wang WN, Pang FF, Chen ZY, et al. Magneto-optical properties and measurement of the novel doping silica optical fibers. Measurement. 2018;**127**:63-67

[21] Kim Y, Ju S, Jeong S, Jang MJ, Kim JY, Lee NH, et al. Influence of gamma-ray irradiation on Faraday effect of Cu-doped germano-silicate optical fiber. Nuclear Instruments and Methods in Physics Research Section B: Beam Interactions with Materials and Atoms. 2015;**344**:39-43

[22] Wen JX, Wang WN, Guo Q , Huang Y, Dong YH, Pang FF, et al. Gamma-ray radiation on magneto-optical property of Pb-doped silica fiber. Inorganic Materials. 2018;**33**(4):416-420

[23] Wei S, Luo YH, Ding MJ, Cai FF, Xiao G, Fan DS, et al. Thermal effect on attenuation and luminescence of Bi/Er Co-doped fiber. IEEE Photonics Technology Letters. 2017;**29**(1):43-46

[24] Yang G, Chen DP, Wang W, Xu YS, Zeng HD, Yang YX, et al. Effects of thermal treatment on broadband near-infrared emission from Bi-doped chalcohalide glasses. Journal of the European Ceramic Society. 2008;**28**:3189-3191

[25] Yang G, Chen DP, Ren J, Xu YS, Zeng HD, Yang YX, et al. Effects of melting temperature on the broadband infrared luminescence of Bi-doped and Bi/Dy co-doped chalcohalide glasses. Journal of the American Ceramic Society. 2007;**90**(11):3670-3672

[26] Dianov EM, Dvoyrin VV, Mashinsky VM, Umnikov AA, Yashkov MV, Gur'yanov AN. CW bismuth fibre laser. Quantum Electronics. 2005;**35**:1083-1084

[27] Puurunen RL. Surface chemistry of atomic layer deposition: A case study for the trimethylaluminum/water process. Applied Physics Reviews. 2005;**97**:121301

[28] George SM. Atomic layer deposition: An overview. Chemical Reviews. 2010;**110**:111-131

[29] Sneck S, Soininen P, Putkonen M, Norin L. A new way to utilize atomic layer deposition-case study: Optical fiber manufacturing. In: Proceedings of AVS - 6th International Conference on Atomic Layer Deposition. 2006

[30] Montiel i Ponsoda JJ, Norin L, Ye C, Bosund M, Söderlund MJ, Tervonen A, et al. Ytterbium-doped fibers fabricated with atomic layer deposition method. Optics Express. 2012;**20**:25085-25095

[31] Dong YH, Wen JX, Pang FF, Chen ZY, Wang J, Luo YH, et al. Optical properties of PbS-doped silica optical fiber materials based on atomic layer deposition. Applied Surface Science. 2014;**320**:372-378

[32] Shang YN, Wen JX, Dong YH, Zhan HH, Luo YH, Peng GD, et al.

Luminescence properties of PbS quantum-dot-doped silica optical fibre produced via atomic layer deposition. Journal of Luminescence. 2017;**187**:201-204

[33] Dong YH, Wen JX, Guo Q , Pang FF, Wang TY. Formation and photoluminescence property of PbS quantum dots in silica optical fiber based on atomic layer deposition. Optical Materials Express. 2015;**5**(4):712-719

[34] Wang Q , Wen JX, Luo YH, Peng G-D, Pang FF, Chen ZY, et al. Enhancement of lifetime in Er-doped silica optical fiber by doping Yb ions via atomic layer deposition. Optical Materials Express. 2020;**10**:2397-2407

[35] Shen YD, Li YW, Li WM, Zhang JZ, Hu ZG, Chu JH. Growth of Bi_2O_3 ultrathin films by atomic layer deposition. Journal of Physical Chemistry C. 2012;**116**:3449-3456

[36] Wang TY, Wen JX, Luo WY, Xiao ZY, Chen ZY. Influences of irradiation on network microstructure of low water peak optical fiber material. Journal of Non-Crystalline Solids. 2010;**356**:1332-1336

[37] Wen JX, Che QQ , Dong YH, Guo Q , Pang FF, Chen ZY, et al. Irradiation effect on the magneto-optical properties of Bi-doped silica optical fiber based on valence state change. Optical Materials Express. 2020;**10**(1):88-98